



Document Document [SAF/OSI/CDOP3/KNMI/SCI/GUI/390](#), NWPSAF-KN-UD-007

Version 1.5

Date 18-01-2021

# Wind Bias Correction Guide

Ad Stoffelen and Jur Vogelzang

KNMI, the Netherlands

## Wind Bias Correction Guide

Ad Stoffelen and Jur Vogelzang

KNMI, the Netherlands

This documentation is maintained within the context of the EUMETSAT Satellite Application Facility on Ocean and Sea Ice (OSI SAF), under the Cooperation Agreement dated 29 June 2011 (CDOP4), between EUMETSAT and the Météo France by KNMI.

This documentation was first developed within the context of the EUMETSAT Satellite Application Facility on Numerical Weather Prediction (NWP SAF), under the Cooperation Agreement dated 29 June 2011 (CDOP2), between EUMETSAT and the Met Office, UK, by one or more partners within the NWP SAF. The partners in the NWP SAF CDOP2 were the Met Office, ECMWF, KNMI and Météo France.

Copyright 2020, EUMETSAT, All Rights Reserved.

Change record			
Version	Date	Author / changed by	Remarks
1.0	Nov 2011	Ad Stoffelen and Jur Vogelzang	First public release
1.1	Apr 2014	Jur Vogelzang	Corrected and extended triple collocation results.
1.2	Apr-Oct 2015	Jur Vogelzang and Ad Stoffelen	Corrected triple collocation results in section 3.2, U10S and geographical biases
1.3	Oct 2016	Jur Vogelzang	Updated triple collocation results
1.4	Sep 2018	Ad Stoffelen	In preparation for the NWP SAF workshop
1.5	Dec 2020	Ad Stoffelen and Jur Vogelzang	Need for geographical model bias correction

---

## Contents

<b>1</b>	<b>Introduction .....</b>	<b>4</b>
1.1	Aims and scope .....	4
1.2	About this document.....	5
<b>2</b>	<b>Scatterometry.....</b>	<b>6</b>
2.1	What does a scatterometer wind represent?.....	6
2.2	What does a NWP surface model wind represent?.....	11
2.3	Surface truth: buoy winds .....	12
<b>3</b>	<b>Biases .....</b>	<b>15</b>
3.1	How to detect global biases? .....	15
3.2	Triple collocation calibration.....	16
3.3	Calibration by regression .....	20
3.4	CDF matching .....	21
3.5	Geographical differences .....	22
3.5.1	ERA* .....	23
3.6	Extreme Winds .....	24
<b>4</b>	<b>Guidance .....</b>	<b>27</b>
	<b>References .....</b>	<b>29</b>
	<b>Useful web sites.....</b>	<b>33</b>

## 1 Introduction

### 1.1 Aims and scope

This guidance document addresses how systematic differences between NWP models and scatterometer wind observations, further referred to as biases, may be estimated and corrected. These biases are relevant for NWP data assimilation and ocean forcing. The purpose of data assimilation is to provide a model state that gives the best match between the most recent model prediction and the observations that became available since the forecast was produced. This state is called the analysis.

Modern data assimilation techniques as Kalman filtering, 3DVar, and 4DVar require good estimates for the random error characteristics of both NWP model and observations, since these error variances determine the relative weight of each of the information sources in the analysis. These techniques are furthermore based on BLUE, Best Linear Unbiased Estimate, and therefore do not deal with biases, either constant or variable. Therefore, wind biases can be detrimental for NWP data assimilation, e.g., negative impacts may occur by decelerating or accelerating flows and thereby filling in or intensifying atmospheric disturbances or lows. Moreover, a NWP model tends to restore its dynamical biases and thus systematic forcing by wind observations in data assimilation tends to be ineffective. It is thus important to correct for biases with respect to the NWP model wind climate. Further note that bias correction schemes for satellite radiances are common in data assimilation to facilitate BLUE by providing consistent satellite and NWP model data; see *Dee* (2005) and references therein or *Dee and Uppala* (2008). In practice best forecast results are obtained when the observations are corrected to fit the model wind climate, even when the biases are caused by model imperfections: consistency appears to be generally more important than absolute calibration in NWP dynamics.

Biases in scatterometer observations are studied in detail (e.g., *Stoffelen*, 1998b; *Vogelzang et al.*, 2011; *Trindade et al.*, 2015). Moored buoys are generally taken as calibration target to establish “surface truth”. This does not at all mean that biases of scatterometer winds against the various NWP models will be minimized in this way. In the next sections we discuss what scatterometer winds and NWP winds represent and how these different representations may lead to biases. We specifically address so-called pseudo biases due to differences in spatial representation of NWP model, scatterometer and buoy winds. Moreover, NWP and scatterometer biases may change with wind speed, direction, time, atmospheric convection and stratification, climate regime, ocean currents, etc.. Actual biases are elaborated in the next sections and remedies discussed.

Several reasons may exist why users wish to perform further bias correction:

- The SAF winds are biased with respect to the winds from a particular NWP model, which is used for the assimilation of the scatterometer winds;

- The scatterometer winds are blended with other wind data sets for a particular user application or service, where calibration does not match.
- The SAF product specifications for product quality are inadequate, for example, a user may wish to use a different spatial sampling, corresponding to a different accuracy and bias (wind biases can be resolution dependent);

A closely related report from the EUMETSAT OSI SAF concerns mainly spatial aspects of high-resolution wind data assimilation (Document SAF/OSI/CDOP3/KNMI/SCI/GUI/388 or NWPSAF-KN-UD-008).

## **1.2 About this document**

This document is written for all users of [Ocean and Sea Ice Satellite Application Facility \(OSI SAF\) scatterometer processors](#) and OSI SAF and [CMEMS](#) scatterometer wind products. It gives the state of the art concerning common NWP model and scatterometer wind error characteristics in terms of resolution, bias, and accuracy, and contains recommendations how to correct for geophysical and geographical biases. The authors hope that this will help the user community to exploit the potential of scatterometer wind data as much as possible. Moreover, the authors much appreciate your feedback.

Within the OSI SAF software is developed for processing scatterometer data over the open ocean to ocean vector winds. This software is freely available in the NWP SAF upon registration, and is also used in the OSI SAF to produce near-real-time ocean vector wind products.

It has been demonstrated that the SAF scatterometer winds are accurate and reliable. Yet, as every measured quantity, these products have their particular error characteristics. Long term monitoring is needed to reveal these characteristics, and this is part of the tasks of the NWP SAF and OSI SAF project teams. Correction for biases in scatterometer winds is considered to be the responsibility of the OSI SAF and performed according to requirements from the broad user community, extending beyond NWP users. For example, requirements are expressed within [EUMETSAT](#) user meetings, the Coordination Group for Meteorological Satellites ([CGMS](#)), Centre for Earth-Observing Satellites ([CEOS](#)) virtual Ocean Vector Winds constellation or the International Ocean Vector Winds Science Team ([IOVWST](#)) for, inter alia, nowcasting, oceanographic or climate applications.

## 2 Scatterometry

### 2.1 What does a scatterometer wind represent?

A scatterometer is a radar instrument that measures the radar cross section of a portion of the Earth's surface (for space-borne scatterometers typically of size 25 km × 25 km) from a number of incidence and/or azimuth angles and/or polarizations. The normalized radar cross section,  $\sigma_0$ , is a geophysical surface property and a measure for the fraction of incident radar radiation scattered back under given azimuth and incidence angle. It is measured by a scatterometer antenna with known antenna gain pattern and distance between radar and scattering surface.

There are two ways of modeling  $\sigma_0$  as a function of the other parameters: empirical and fundamental. In the fundamental approach wave generation (short waves) by wind and radar backscatter from the ocean surface are modeled to yield  $\sigma_0$  (e.g., *Fois, 2015*). On the other hand, the empirical approach assumes some form of  $\sigma_0$  as a function of the other parameters with a number of coefficients that are fitted to the observations. The outcome of the two approaches is the same: a prescription of how to calculate  $\sigma_0$  as a function of wind speed and direction, measurement geometry, radar properties, etc. This function is called the Geophysical Model Function (GMF). The empirical approach has two main advantages over the more fundamental approaches (given the present state of the fundamental algorithms): the radar cross section is calculated faster and it is calculated more accurately. This makes the empirically-derived GMFs best suited for application in scatterometer wind retrieval (*Stoffelen et al., 2017*).

The radar cross section Geophysical Model Function is defined as

$$\sigma_0 = GMF(U_{10S}, SST, \phi, \theta, p, \lambda) , \quad (1)$$

with  $U_{10S}$  the stress-equivalent wind speed (*de Kloe et al., 2017*),  $\phi$  the wind direction w.r.t. beam pointing azimuth  $\varphi$ , SST Sea Surface Temperature,  $\theta$  the beam incidence angle,  $p$  the radar beam polarization and  $\lambda$  the microwave wavelength. An example is shown in figure 1.

The radar cross section is a property of the surface itself. It is a measure of the surface roughness,  $z_0$ , and related to the wind stress vector,  $\boldsymbol{\tau}$ . This is in turn related to the friction wind velocity,  $u_*$  or  $\mathbf{u}_*$  in vector notation. The surface wind at 10 m anemometer height,  $U_{10}$ , depends on  $u_*$  and the temperature difference between the ocean and the overlying air. To avoid the latter dependency of scatterometer winds, reference winds from buoys and NWP models that are used for validation are processed at equivalent neutral stability, i.e., using equal temperature of air and sea (e.g., *Hersbach, 2010a*). Moreover, the reference  $U_{10S}$  winds take into account air mass density effects that are relevant in the momentum exchange between air and water. In the following equations and following *Portabella and Stoffelen (2009)*, also ocean currents  $U_C$  are accounted for, as a scatterometer measures the wind relative to the moving water surface.

$$U_{10} - U_C = \frac{u_*}{\kappa} \left[ \ln \left( \frac{10}{z_0} \right) - \psi \left( \frac{10}{L} \right) \right], \quad (2)$$

$$z_0 = 0.11 \frac{\nu}{u_*} + \alpha \frac{u_*^2}{g}, \quad (3)$$

$$\boldsymbol{\tau} = \rho u_* \mathbf{u}_*, \quad (4)$$

$$U_{10S} = \sqrt{\frac{\rho}{\rho_0}} \cdot \frac{u_*}{\kappa} \left[ \ln \left( \frac{10}{z_0} \right) \right] = \sqrt{\frac{\tau}{\rho_0}} \cdot \frac{1}{\kappa} \ln \left( \frac{10}{z_0} \right), \quad (5)$$

where  $\kappa = 0.41$  is the von Karman constant,  $z_0$  is the roughness depth (also called roughness length),  $\psi$  is the stability function (positive, negative, and null, for unstable, stable, and neutral atmospheric stability, respectively) and  $L$  is the Monin-Obukhov length, which includes the effects of temperature and moisture fluctuations on buoyancy.  $\rho$  is the air mass density with reference value  $\rho_0 = 0.1225 \text{ kg m}^{-3}$ ,  $\nu$  is the air kinematic viscosity ( $1.5 \cdot 10^{-5} \text{ m}^2/\text{s}$ ),  $g$  is the gravitational acceleration at the Earth's surface ( $9.8 \text{ m/s}^2$ ), and  $\alpha$  the dimensionless Charnock parameter. Note that

- 1)  $U_{10S}$  only depends on the variables  $u_*$ ,  $z_0$  and  $\rho$ , where the former two are dependent; these variables are computed from buoy or ECMWF winds;
- 2) To go from the surface variables  $u_*$ ,  $z_0$  to  $U_{10S}$ , stability is taken neutral in the lowest 10m;
- 3) The effect of air mass density to create ocean roughness is represented (see Figure 1);
- 4)  $U_{10S}$  is defined with respect to the moving ocean surface as the ocean current  $U_C$  is accounted for; note however, that accurate  $U_C$  information is generally not available to correct ECMWF and buoy winds (*Belmonte and Stoffelen, 2019*).

The GMF for ASCAT is called CMOD. The current version is CMOD7 (*Stoffelen et al., 2017*). It does not depend on SST. The radar cross section measurements typically have errors of 5%, while  $\varphi$ ,  $\theta$ ,  $\rho$ , and  $\lambda$  are known very accurately. Given radar cross section data at multiple azimuths as measured by a scatterometer, the GMF is inverted to compute the local wind vector (or wind vector probability distribution; see *Stoffelen and Portabella (2006)*). See also *Portabella (2002)*, and *Stoffelen (1998a)*, who describe the scientific background to the non-linear Bayesian wind retrieval and processing.

The Ku-band GMF used at KNMI is inherited from the NSCAT instrument as it covers a wide incidence angle range. For Ku-band wavelengths, dissipation due to viscosity appears important, as RapidScat winds are biased with respect to collocated ASCAT-B winds and with respect to other wind references, such as in situ and NWP winds as a function of SST (*Wang et al., 2016*). Figure 2b shows the bias between RapidScat and ASCAT-B as a function of SST and wind speed. Wind speed is estimated by taking the mean of the ASCAT and RapidScat retrievals, as they are assumed to be equally accurate. A linear SST dependence emerges, but which depends on speed. The highest SST dependency occurs around a speed of 7 m/s, with lower dependency in the seas dominated by both low and high winds, which latter are dominated by wave breaking processes, while for low winds no breaking occurs. This effect is being incorporated in the Ku-band wind retrieval in the SAFs.

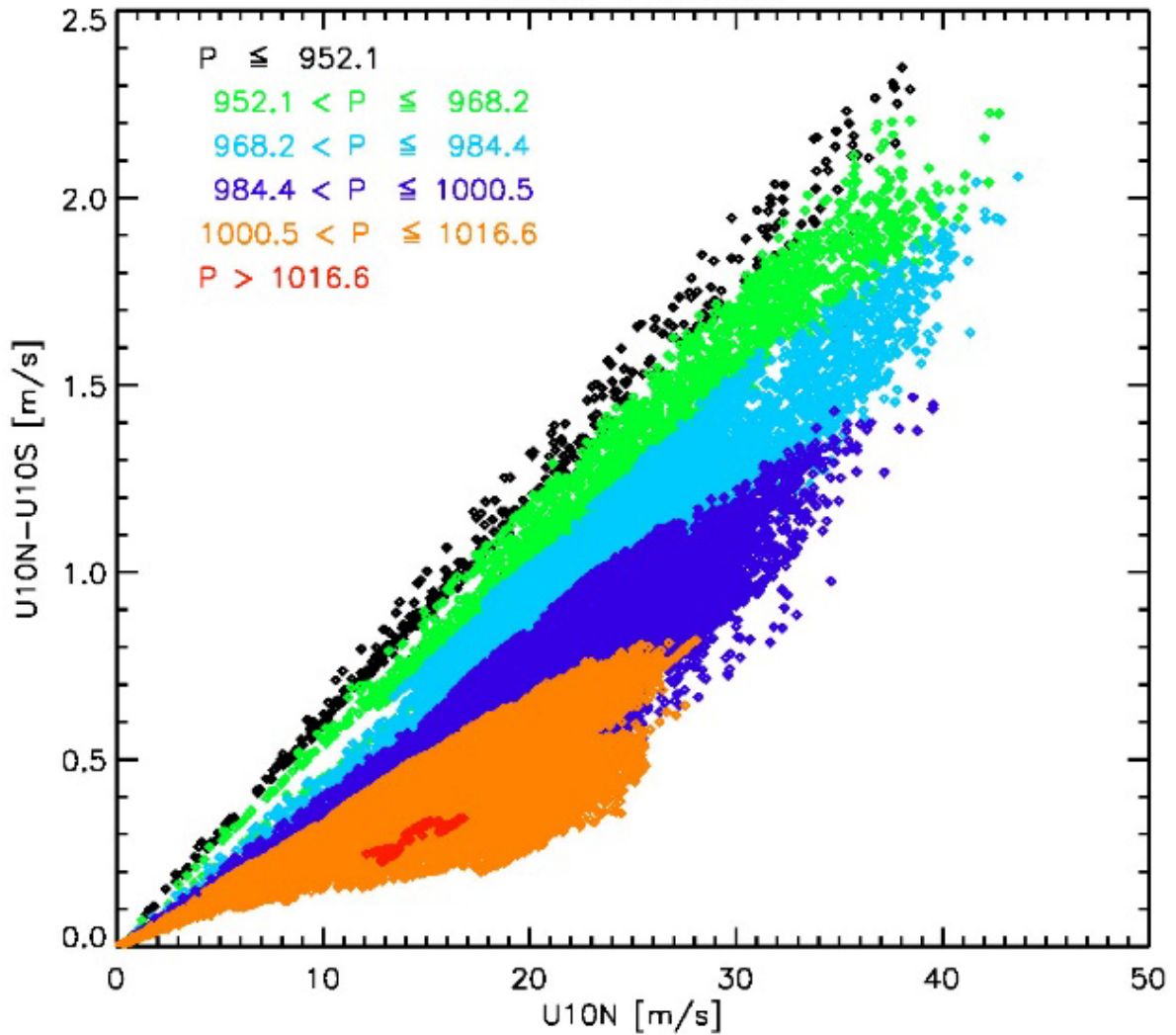
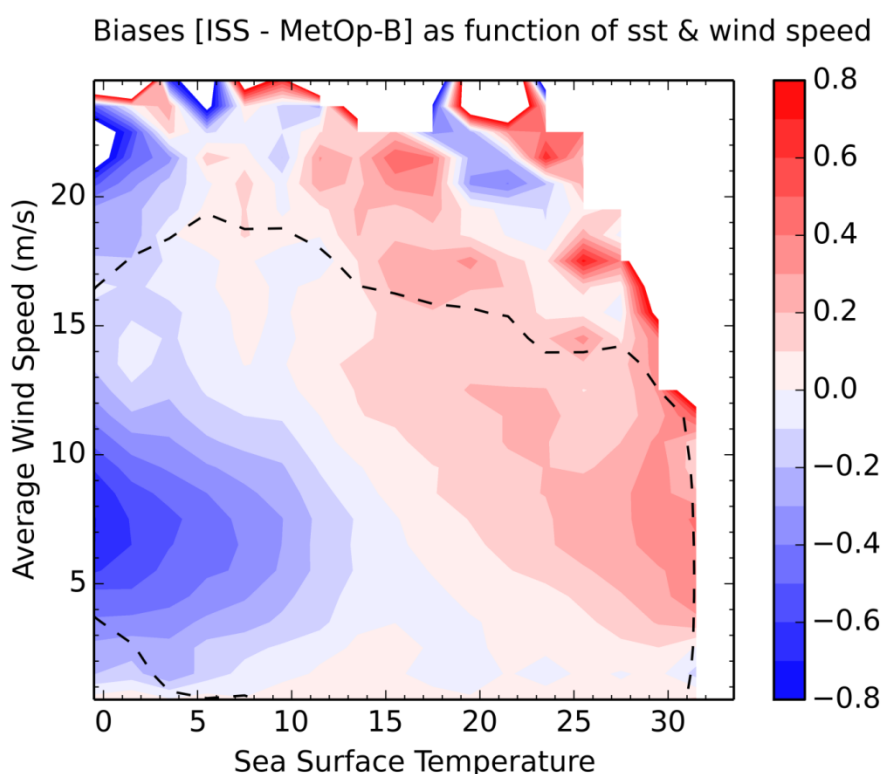


Figure 1 The effect of air mass density in hurricanes. Difference between  $U_{10N}$  and  $U_{10S}$  with respect to  $U_{10}$ . Color coded are different surface pressure classes. (from <https://www.eumetsat.int/CHEFS>)



**Figure 2** RapidScat minus ASCAT wind speed bias in m/s as a function of SST and average wind speed;  
 The dashed line bounds an area with sufficient sampling. (*courtesy Z. Wang*)

A few remarks can be made concerning further systematic effects related to scatterometer winds:

- A scatterometer wind is measured w.r.t. the current and not w.r.t. an earth-fixed frame like buoy and NWP winds. In the Gulf Stream or the Kuroshio current, the discrepancy may be occasionally as large as 1 m/s in speed;
- Roughness is caused by air-sea momentum exchange (stress) which depends on atmospheric mass  $\rho$ , where Eq. (5) suggests such dependency (*de Kloe et al., 2017*);
- While it plays a role in air-sea momentum exchange, ocean mass density variations may be ignored, since these vary only by a per mille over the globe (e.g., [http://en.wikipedia.org/wiki/Water\\_\(molecule\)#Density\\_of\\_water\\_and\\_ice](http://en.wikipedia.org/wiki/Water_(molecule)#Density_of_water_and_ice) and NOAA World Ocean Atlas);
- The momentum exchange and small-scale ocean roughness at a given stress-equivalent wind may depend on variations in sea state. *Portabella and Stoffelen (2009)* found no such dependency in a statistical assessment using the ECMWF WAM model wave state parameters. In extreme conditions, particularly near the coast, such effects are considered plausible however. On the other hand, it has been noted that some of these conditions are flagged by the scatterometer Quality Control (QC) at KNMI (*Verhoef et al., 2019*).

The following effects are also known for their systematic behavior:

- Contamination by land and/or sea ice. Land and sea ice have a much larger radar cross section than the ocean surface, so land or sea ice contamination of a cell may lead to overestimation of the wind speed. Quality Control prevents such contamination (e.g., *Belmonte et al., 2011*).
- Presence and intensity of rain. Microwave radiation at Ku band is scattered into all directions by large rain drops in the atmosphere and therefore less ocean signal is received back than in the absence of rain. On the other hand, rain clouds cause backscattering, leading to overestimation of the wind. These two effects are substantial at Ku-band wavelengths (NSCAT, SeaWinds, OSCAT, RapidSCat, HY2A/B/C, ScatSat, CFOSAT; *Nie and Long, 2008*) and intense rain provides an artificial wind speed of about 15 m/s. However, KNMI QC is quite effective in removing rain-contaminated winds by using MSS and 2DVAR (*Xu et al., 2020*). Splashing rain on the ocean surface disturbs the radar cross section too, and could enhance it at low winds and reduce it at high winds. SAR images at C band indicate that these effects are rather spatially and temporally limited and negligible (*Alpers et al., 2016*). As a result, C band wind measurements appear rather immune for rain contamination (ERS, ASCAT; *Portabella et al., 2011; Lin et al., 2015; King et al., 2017*).

Scatterometer processing starts with defining a regular grid of Wind Vector Cells (WVCs) on the Earth's surface. The area of a WVC is larger than the area over which a single radar measurement is performed. Next, for each measurement geometry all individual radar measurements centered within a WVC are averaged. This results in a gridded  $\sigma_0$  product in which each WVC contains exactly one  $\sigma_0$  value per antenna view type. The averaging process reduces the speckle noise (measurement error) that is inherent in radar observations to typically 5%. At the lower winds sea surface roughness is the most variable and variations within a WVC cause additional geophysical variability and noise (*Portabella and Stoffelen, 2006*), but with rather limited effect on wind vector accuracy.

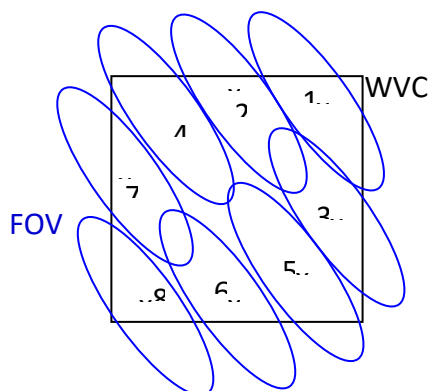


**Figure 3** Averaging the radar views (FOV; blue ellipses) in the WVC (black square).

Scatterometer wind processing starts with the gridded  $\sigma_0$  product. The retrieved wind is therefore representative for the WVC. The WVC size determines the spatial resolution of the wind field, i.e., the size of the smallest wind feature visible. In practice the individual radar measurements do not cover the WVC exactly, nor are they spread homogeneously. Such effects are small and generally neglected. Multiple views in varying antenna geometry, notably in azimuth, are needed to resolve the wind vector. Due to the varying antenna orientation (see Figure 3), the area sampled in a given WVC (Cumulative Spatial Response Function, CSRF) is not identical in the different views (*Vogelzang and Stoffelen, 2017*). Wind variability in the WVC area therefore causes noise in the wind retrieval, contributing to the geophysical noise. The combination of speckle and geophysical noise results in an estimated random wind vector RMS error of about 0.5 m/s (*Portabella and Stoffelen, 2006*).

In order to further improve scatterometer wind biases, the following activities are ongoing:

- Ocean calibration to improve consistency between scatterometer missions using cone metrics (*Belmonte et al., 2017*);
- GMF improvements which are expected to benefit consistency of wind calibration across the swath and wind direction retrieval, particularly at winds below 4 m/s and improved in situ references above 20 m/s ([EUMETSAT CHEFS project](#));
- Study of geophysical effects, such as those concerned with air-sea momentum exchange, e.g., effects of waves or SST in generating ocean roughness;
- QC development in variable wind and rain conditions, near the coast and near the ice edge;
- Study of bias and wind variability effects due to spatial resolution, i.e., concerning wind PDF variation as a function of spatial resolution, effects of noise and the non-linear wind retrieval function (e.g., *Wang et al., 2020*).

The vector RMS error of scatterometer winds is estimated to be 1.0 m/s with biases generally below a few  $10^{\text{th}}$  of a m/s (*Vogelzang et al., 2012*), while spatial characteristics are those expected of atmospheric turbulence (e.g., *King et al., 2014*). Near moist convection, scatterometer winds appear quite reliable (*Lin et al., 2015; King et al., 2017*).

## 2.2 What does a NWP surface model wind represent?

A NWP model calculates meteorological quantities like wind on a regular grid. The equations use derivatives in space and time and only structures defined over several grid points are propagated well. In NWP grid distance is commonly referred to as model resolution, but spatially resolved structures over the open oceans are usually about 5-10 times larger (*Skamarock, 2005*). NWP model fields are propagated in discrete time steps and the model values are also representative for a time window of several time steps. This poses, of course, limits to the effective spatial and temporal resolution of the model fields. The size of these limits depends on the model characteristics, e.g., horizontal and vertical diffusion schemes and closure of the dynamical equations. In particular, the representation of 3D turbulence and associated convection on scales below 500 km (*Nastrom and Gage, 1985*) is generally poor in global NWP models (*King et al., 2017*). Given their high accuracy and low bias,

scatterometer vector winds collocated with NWP model wind fields are ideal to investigate spatial and temporal NWP model error properties (*Belmonte & Stoffelen, 2019; Trindade et al., 2020*).

The NWP surface wind vector depends on how the surface layer processes are described in the model (cf. eq. 2-4) and on the representation of boundary layer processes and (moist) convection. Notable aspects are:

- Stress-equivalent surface winds ( $U_{10S}$ ) are computed from the NWP model friction velocity, which cannot be directly calibrated. In fact, the NWP model  $U_{10S}$  is validated against buoys when stability information has been measured (e.g., *Portabella and Stoffelen, 2009*). NWP model stability tends to be too neutral (e.g., *Hersbach, 2010a, Sandu et al., 2013*). When the advected air is much warmer than the ocean, the situation is called stable. Under such conditions the wind profile over the ocean surface changes, leading to reduced surface wind and increased turning of the wind with height. The coupling of NWP surface winds with the free tropospheric winds is generally too large in stable conditions (*Belmonte & Stoffelen, 2019*), leading to strength and direction biases (often > 10 degrees) in the surface stress vector (eq. 4). When the ocean is warmer than the overlying air the situation is called unstable. Underestimated instability has generally a smaller effect on the surface stress vector error than underestimated stability, but wind variability due to moist convection is often much underestimated (*Lin et al., 2015; King et al., 2017*). Several different NWP parameterizations for the wind profile exist with differences in momentum flux of up to 30%, and also 10-m wind biases of NWP models can be locally and seasonally large at 20% percent (*Belmonte & Stoffelen, 2019*). To our knowledge, this statement includes NWP models with surface layer dependency on sea state (*de Kloe et al., 2017*), but further feedback from the user community would be welcome here.
- Drag parameterization is uncertain at high winds and in-situ wind references are mutually inconsistent; more work is needed to understand these in-situ references ([EUMETSAT CHEFS project](#)).
- NWP models do generally not describe ocean current, although developments in this direction are under way in several centers. Moreover, skillful deterministic ocean current modeling is still in its infancy. Without current representation, the relative motion between free troposphere and surface will be in error, e.g., too fast when a local current exists in the direction of the atmospheric flow. In this case and in case of moderate or high winds the surface stress and the roughness depth will be exaggerated. Subsequently  $U_{10S}$  will be estimated too high according to eq. (2). It is clear that biases result in NWP model  $U_{10S}$  due to ocean current misrepresentation, but with amplitude depending on NWP model surface layer parameterization (*Belmonte & Stoffelen, 2019*).

## 2.3 Surface truth: buoy winds

Both scatterometer and NWP model winds lack calibration. Conventional wind sensors are calibrated well for low, modal and high winds, however, and are generally used as calibration

standard for both scatterometer and NWP winds. In particular moored buoys are reliable platforms dedicated to atmospheric and oceanographic measurement.

A number of moored buoys measure the wind speed and direction, not disturbed by the platform and corrected for platform motion, together with a number of other parameters. If these include air and sea temperatures, it is possible to convert the measured wind vector to a stress-equivalent wind vector at 10 m anemometer height and compare to scatterometer winds. Buoy winds are commonly given as averages over 10 minutes. Note that buoys give time-averaged winds at a fixed location, while scatterometers give a spatially averaged wind at a certain time. A typical wind speed of 7 m/s averaged over 10 minutes (600 s) corresponds to a track in one dimension of about 4 km length and a spatial scale of about 2 km. This is about one order of magnitude smaller than the typical scatterometer spatial resolution. Thus, moored buoys and NWP and scatterometer winds each have a different spatial representation. It is important to note in this respect that spatial averaging of the wind field leads to a narrowing of the wind speed PDF and one would thus expect less extreme winds in a NWP data set than in a buoy wind data set. A narrower wind speed PDF corresponds to a lower mean wind of the wind PDF. Spatial averaging thus leads to a bias in the wind speed (reduction of the mean) w.r.t. the original data. It is clear that spatial representation has to be taken into account in calibration<sup>1</sup>.

Moored buoy platforms do not reach 10-m height generally. Therefore, actual roughness depth and stress need to be estimated at the buoy measurement site and these be represented as stress-equivalent 10-m winds,  $U_{10S}$ , in order to represent the scatterometer data. Although roughness depth and stress vector PDFs do depend on the surface layer parameterization,  $U_{10S}$  appears rather independent of the parameterization (*Portabella and Stoffelen, 2009*).

The buoy wind measurements are w.r.t. an earth-fixed reference frame and thus in case of ocean current do not provide an appropriate reference to scatterometer winds, nor provide good input for air-sea fluxes which essentially depend on the relative motion of air and sea. For the main ocean currents biases up to 1 m/s may occur and may be corrected at some buoy locations (*Kelly, 2001; Belmonte & Stoffelen, 2019*).

Buoy wind sensors need calibration and maintenance. To address performance anomalies, monitoring and QC are in place at several centers (e.g., *Bidlot et al., 2002*). These schemes prevent instrumental errors to propagate into calibration parameters, but, on the other hand, somewhat affect geophysical and spatial sampling.

Sampling biases may further occur when the data set used is not representative for the global wind climate. High-quality buoy measurements, for instance, are concentrated in the tropical

---

<sup>1</sup> One may increase temporal averaging to match spatial representation, i.e., using Taylor's frozen turbulence hypothesis, but we note that a fixed temporal averaging implies variable spatial representation as a function of wind speed (3 hours averaging corresponds to a 20 km stretch at 2 m/s and a 200 km stretch at 20 m/s). For this reason we do not recommend this approach (but see *Lin et al., 2014*).

oceans and along the coasts of North America and Europe (see Figure 4). Therefore, calibration results may not be fully representative of the global ocean conditions and be geographically biased towards tropical and coastal wind distributions (*Stoffelen and Vogelzang, 2015*).

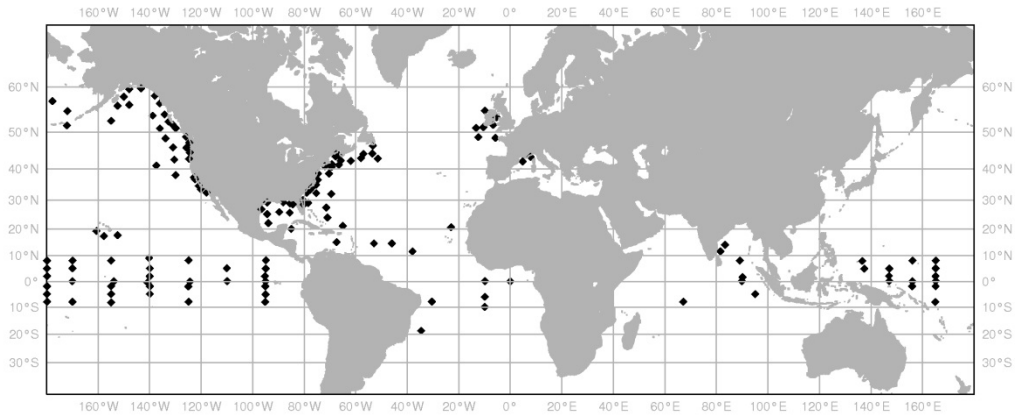


**Figure 4** Irregular global distribution of moored buoys measuring high-quality winds.

## 3 Biases

### 3.1 How to detect global biases?

Biases show up when plotting the difference between scatterometer wind and model wind. A number of such plots is made available on the web. The NWP SAF web page at [nwp-saf.eumetsat.int/site/monitoring/](http://nwp-saf.eumetsat.int/site/monitoring/) provides links to monitoring pages of scatterometer differences with ECMWF, UKMO, and KNMI NWP models; so-called *o-b* and *o-a* differences with NWP background and analysis fields, respectively. These differences provide monitoring information on scatterometers and models. Also many error studies are published in the scientific literature and presented at IOVWST meetings for example (<http://coaps.fsu.edu/scatterometry/meeting/past.php>).

Systematic differences in winds occur due to

- 1) System calibration errors; for example, speed-dependent biases will show up as geographically- and time-dependent biases, since the wind vector PDF is geographically and time dependent due to weather and climate;
- 2) Differences in spatial representation; local wind PDFs (buoys) have more extreme values than area-mean wind PDFs (NWP, scatterometer);
- 3) Undetermined geophysical dependencies, e.g., currents, wind variability (e.g., downbursts in moist convection, turbulence), SST, sea state, etc.;
- 4) So-called pseudo biases in wind speed due to non-linear transformation of random component errors (*Stoffelen, 1998b*);

Only categories 1 and 3 are systematic errors that need to be corrected for BLUE wind component data assimilation, while categories 2 and 4 need to be acknowledged, but are not incompatible with BLUE wind components when treated appropriately (as representativeness error).

Concerning 1), for statistical calibration of wind vector components, two methods are distinguished here:

- Triple collocation. This is the most general, but also the most elaborate method. It yields global (linear) calibration coefficients and error variances for three collocated data sets; PDF matching may be used subsequently for non-linear calibration;
- *o-b* regression. Under some assumptions discussed below, also *o-b* regression may give useful results.

Regression techniques are widely used to calibrate data sets. Regression will generally lead to useful results when the dynamic range of the variables is large as compared to the errors involved. For wind components, however, the dynamic range is typically 5 m/s, while random errors are typically 1 m/s, i.e., not negligible w.r.t. the dynamic range. In such cases, the regression result will critically depend on the random error assumptions, which assumptions

often will be implicit rather than explicit. Moreover, the spatial representation error has to be well taken into account in the random error attribution. We will now illustrate the two methods. Note that data assimilation systems require BLUE wind components and usually specify an estimated random wind component error that is constant. We note that wind components generally behave like variables with constant random error due to the fact that a large proportion of the NWP and observation errors are due to wind variability effects. Wind variability effects on scales below 500 km are mainly governed by 3D turbulence, which in turn is well described as normal variations in wind component on the different scales (*King et al., 2014*). In fact, variations in wind speed and wind direction are more complex functions of 3D turbulence and speed and direction errors therefore more difficult to characterize (see also *Stoffelen, 1998*).

## 3.2 Triple collocation calibration

### Method

The triple collocation method assumes that three systems (buoys, scatterometer, and model background in the case considered here) all give information on the true value  $t$ . The buoy is chosen as absolute reference relative to which the other systems are calibrated. Assuming that the buoy is free of bias (i.e., free of systematic errors) and that linear calibration suffices for the other two systems, the values  $w$  measured by the different systems satisfy

$$\begin{aligned} w_{buoy} &= t + \delta_{buoy} \\ w_{scat} &= \alpha_{scat}t + \beta_{scat} + \delta_{scat} \\ w_{back} &= \alpha_{back}t + \beta_{back} + \delta_{back} \end{aligned} \tag{6}$$

with  $\alpha$  and  $\beta$  the calibration coefficients and  $\delta$  the random measurement error. Since most errors will be due to speed scaling effects and wind components can be both positive and negative, the  $\beta$  calibration coefficients are generally very small and may be ignored.

Forming equations for all first and second statistical moments results in a set of equations that are further simplified by the following assumptions on the error characteristics:

- Linear calibration by  $\alpha$  and  $\beta$  is sufficient over the whole range of measurement values considered for scatterometer and NWP winds;
- The reference measurement values are unbiased (see above);
- The measurement errors have constant variance over the whole range of measurement values; this is generally corroborated by combined PDF's of two wind data sets which show a rather constant width of the difference distribution as a function of wind component strength;
- The measurement errors are uncorrelated with each other since they are realized independently; spatial representation errors may concern similar spatial scales and are treated separately;

- The measurement errors are uncorrelated with the measurement values; in fact, any variation that is common (correlated) in the three systems is interpreted as a dependent realization and caused by the underlying true wind field. The spatial scales represented in  $t$  are thus determined by the deterministic scales in the NWP model, as this is generally the coarsest among the three systems.

Since both the scatterometer and buoy have better effective resolution than the NWP system, they both may resolve true wind variance that is not resolved by the NWP winds. This wind variance will be part of both the spatial representation error of the scatterometer and buoy, and therefore be a correlated part of the observation error. Some subtleties are involved in handling the correlated part of the spatial representation error, see *Stoffelen (1998)*. The following example uses representation errors calculated from wind spectra, see *Vogelzang et al. (2011)*.

Under these assumptions the error variances  $\langle \delta^2 \rangle$  and the calibration coefficients can be solved from equations (6), after which calibration may be performed as follows:

$$\begin{cases} w_{scat}^{cal} = \alpha_{scat}^{-1} w_{scat} \\ w_{back}^{cal} = \alpha_{back}^{-1} w_{back} \end{cases} \Rightarrow w_{scat}^{NWP} = \frac{\alpha_{back}}{\alpha_{scat}} w_{scat} , \quad (7)$$

with superscript *cal* referring to calibration w.r.t. the buoys and superscript *NWP* referring to calibration w.r.t. the NWP model (background) wind climate (following BLUE).

## Data sets

- Buoy measurements not blacklisted by ECMWF (see Figure 4);
- ECMWF or ERA-interim forecast;
- NRT scatterometer data (from OSI SAF, with ECMWF background):
  - ASCAT-A-coastal, September 1, 2010 - August 31, 2016
  - ASCAT-A-12.5, October 1, 2008 - April 28, 2015
  - ASCAT-A-25, April 1, 2007 - August 31, 2016
  - ASCAT-B-coastal, January 11, 2012 - August 31, 2016
  - ASCAT-B-25, January 11, 2012 - August 31, 2016
  - ASCAT-C-coastal, January 08, 2019 - August 31, 2020
  - ASCAT-C-25, January 08, 2019 - August 31, 2020
  - OSCAT-50, January 2, 2012 - February 20, 2014
  - RapidSCAT-25, November 7, 2014 - August 19, 2016
  - RapidSCAT-50, November 7, 2014 - August 19, 2016
  - ScatSat-25, January 20, 2017 - August 31, 2020

- ScatSat-50, January 20, 2017 - August 31, 2020
- SeaWinds-KNMI-25, November 1, 2007 - November 23, 2009
- SeaWinds-KNMI-100, November 1, 2007 - November 23, 2009
- Reprocessed scatterometer data (with ERA-interim background)
  - ASCAT-A-coa January 1, 2007 - March 31, 2014
  - ASCAT-A-25 January 1, 2007 - November 30, 2017
  - OSCAT-25 December 15, 2009 - February 20, 2014
  - OSCAT-50 December 15, 2009 - February 20, 2014
  - SeaWinds-KNMI-25 July 19, 1999 - November 21, 2009
  - SeaWinds-KNMI-50 July 19, 1999 - November 21, 2009

## Results

Let  $u^{cal} = a_u u + b_u$  and  $v^{cal} = a_v v + b_v$  with  $(u, v)$  the wind components from the OSI SAF wind product and  $(u^{cal}, v^{cal})$  the linearly calibrated wind. The calibration constants  $a$  and  $b$  are given in table 1 below for the various scatterometer wind products and for the collocated ECMWF forecast.

**Table 1 Triple collocation calibration coefficients with respect to buoys.  $b$  in  $m s^{-1}$ .**

Dataset	Scatterometer				ECMWF			
	$a_u$	$b_u$	$a_v$	$b_v$	$a_u$	$b_u$	$a_v$	$b_v$
ASCAT-A-coastal	0.998	-0.07	1.005	0.00	1.037	-0.11	1.077	-0.10
ASCAT-A-12.5	1.003	-0.10	1.010	+0.03	1.042	-0.18	1.082	-0.08
ASCAT-A-25	1.002	-0.08	1.003	-0.01	1.015	-0.13	1.045	-0.10
ASCAT-B-coastal	0.991	-0.06	1.003	-0.02	1.037	-0.07	1.078	-0.12
ASCAT-B-25	0.988	-0.07	0.999	-0.04	1.019	-0.05	1.065	-0.13
ASCAT-C-coastal	0.999	-0.10	1.007	-0.07	1.020	-0.17	1.059	-0.16
ASCAT-C-25	0.992	-0.11	1.003	-0.10	1.006	-0.13	1.050	-0.17
OSCAT-50	1.000	-0.06	0.954	+0.05	1.005	-0.14	1.040	-0.07
RapidSCAT-25	0.989	-0.08	0.989	-0.03	1.024	-0.10	1.040	-0.10
RapidSCAT-50	0.982	-0.08	0.974	-0.01	1.013	-0.12	1.026	-0.08
SeaWinds-KNMI-25	1.048	-0.23	1.030	-0.01	1.020	-0.33	1.052	-0.07
SeaWinds-KNMI-100	1.024	-0.22	1.017	0.00	1.017	-0.35	1.044	-0.06
Rep ASCAT-A-Coastal	1.000	-0.12	1.013	+0.03	1.057	-0.23	1.096	-0.07
Rep ASCAT-A-25	0.991	-0.10	1.002	-0.02	1.029	-0.15	1.073	-0.07
Rep OSCAT-25	0.999	-0.10	0.976	+0.03	1.016	-0.19	1.052	-0.03
Rep OSCAT-50	0.984	-0.12	0.978	+0.03	1.007	-0.19	1.035	-0.02
Rep SeaWinds-KNMI-25	0.995	-0.15	0.983	+0.02	1.016	-0.28	1.054	-0.03
Rep SeaWinds-KNMI-50	0.989	-0.19	0.977	+0.03	1.011	-0.30	1.047	-0.03

The error standard deviations are given in table 2 below. The numbers are valid for the calibrated wind components (using the calibration coefficients given above) at the scale of the ECMWF model (for the OSI SAF NRT products) or ERA-interim (for the reprocessed products). See *Vogelzang et al. (2011)* for a discussion of these values. Interestingly, the buoy data have large random wind errors, while it constitutes the best calibrated and most direct winds. This is obviously due to the spatial representation error corresponding to the turbulent wind scales observed by the buoys, but not by the scatterometer and NWP model.

**Table 2 Error standard deviations of buoy and scatterometer observation errors and ECMWF model error at the scale of the ECMWF model in  $\text{m s}^{-1}$ .**

Dataset	Buoy		ECMWF		Scatterometer	
	$\varepsilon_u$	$\varepsilon_v$	$\varepsilon_u$	$\varepsilon_v$	$\varepsilon_u$	$\varepsilon_v$
ASCAT-A-coastal	1.15	1.17	1.39	1.46	0.66	0.83
ASCAT-A-12.5	1.14	1.18	1.46	1.53	0.66	0.80
ASCAT-A-25	1.19	1.24	1.30	1.38	0.55	0.68
ASCAT-B-coastal	1.15	1.17	1.37	1.44	0.65	0.82
ASCAT-B-25	1.17	1.22	1.24	1.32	0.51	0.64
ASCAT-C-coastal	1.07	1.11	1.29	1.37	0.63	0.75
ASCAT-C-25	1.09	1.18	1.17	1.26	0.41	0.46
OSCAT-50	1.41	1.48	0.98	1.08	0.78	0.65
RapidSCAT-25	1.31	1.39	1.10	1.06	0.82	0.88
RapidSCAT-50	1.38	1.46	1.01	0.98	0.66	0.69
SeaWinds-KNMI-25	1.39	1.44	1.20	1.28	0.79	0.63
SeaWinds-KNMI-100	1.50	1.53	1.19	1.28	0.98	0.73
Rep ASCAT-A-coa	1.16	1.17	1.74	1.79	0.63	0.76
Rep ASCAT-A-25	1.19	1.23	1.52	1.59	0.45	0.57
Rep OSCAT-25	1.40	1.43	1.31	1.39	0.80	0.70
Rep OSCAT-50	1.48	1.52	1.19	1.28	0.61	0.49
Rep SeaWinds-KNMI-25	1.42	1.42	1.31	1.34	0.64	0.55
Rep SeaWinds-KNMI-50	1.52	1.50	1.23	1.27	0.45	0.41

Further note that the better resolution ASCAT products ASCAT-A-coastal, ASCAT-A-12.5, and ASCAT-B-coastal show similar errors for the buoy and the ECMWF model, but larger error for the scatterometer than the ASCAT-A-25 and ASCAT-B-25 products. This is mainly due to the spatial representation error variance that increases from about 0.4 to 0.6  $\text{m}^2/\text{s}^2$  when going from the 25 to the 12.5-km product, due to the poorer resolution of the ECMWF model (see *Vogelzang et al., 2011*). However, the representativeness errors decreases in time because of gradual improvements of the ECMWF model spectrum, notably from 2019 onwards. This may explain that all errors for ASCAT-C are lower than those of the corresponding ASCAT-A and ASCAT-B products. Since the RapidScat-25 and SeaWinds-KNMI-25 products are smoother than the ASCAT 25-km products, they have a lower spatial representation error, but that is compensated by a larger instrument error.

Finally, note that the 25-km KNMI SeaWinds product has smaller error than the 100-km KNMI SeaWinds product, whereas for all other sensors the product at larger grid size has smaller

error. This is due to the fact that the 25-km NRT product has been processed with the Multiple Solution Scheme (MSS) which takes the full wind PDF into account, whereas the 100-km product has been processed with the traditional scheme allowing at most four solutions [Vogelzang *et al.*, 2009]. As result, the 25-km product has superior noise reduction characteristics. The reprocessed OSCAT and SeaWinds products were all processed with MSS, and the 25 km products has larger error than the 50 km products. The latter products are spatially smoothed by MSS and seemingly spatially most representative of the ECMWF model<sup>2</sup>.

### 3.3 Calibration by regression

#### Method

When applying standard regression methods on differences between observed (scatterometer) and model winds, one must be cautious as to how the errors are handled. Most regression methods implicitly assume that all errors are contained in the dependent variable while  $o$  and  $b$  errors are of similar size (see table 2), but this will cause errors as depicted in Figure 5.

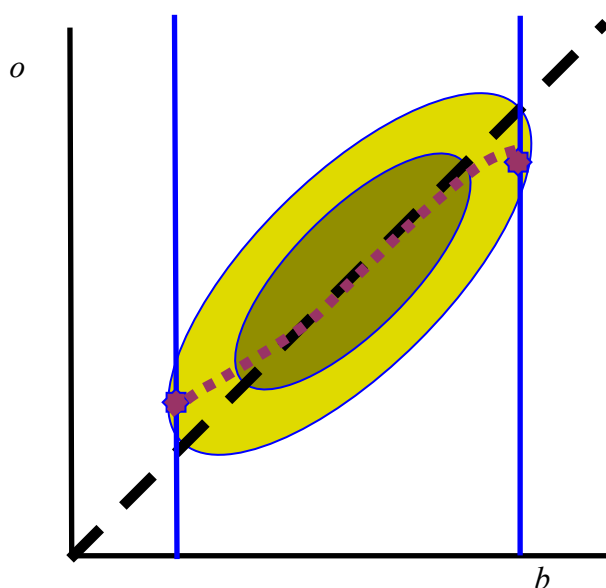


Figure 5 Bivariate  $o$  and  $b$  distribution, showing (dashed) the mean  $o$  as a function of  $b$ .

In Figure 5 the observations are perfectly calibrated (dashed black curve) and dispersed due to  $o$  and  $b$  errors (yellow data density colors). However, when a regression routine assumes all errors to be contained in  $o$ , then the average for low values of  $b$  (red dot on the left-hand-

<sup>2</sup> See also the EUMETSAT NWP SAF high-resolution wind data assimilation (Document NWPSAF-KN-UD-008).

side blue line) will lie above the true calibration curve. Similarly, the calculated average  $\langle o|b \rangle$  at high values of  $b$  (red dot on right-hand-side blue line) will be too low. As a result, regression would yield something like the red dotted curve. In fact, a different regression is obtained when average  $b$  values are computed for given  $o$ ,  $\langle b|o \rangle$ , implicitly assuming perfect  $o$  with no random error.

If, however, one can safely assume that  $o$  and  $b$  have the same random error distribution, which is a more reasonable assumption than assuming either one has no error, one may apply standard regression to  $o - b$  versus  $(o + b)/2$ , as shown in Figure 6. Now standard regression will not introduce large spurious biases. One may also bin the data in  $o + b$  values, as indicated by the blue lines and the yellow arrows, and obtain a non-linear calibration curve by calculating the average in each bin. In this way, calibration issues for low and/or high winds will become visible.

More sophisticated regression methods take the error in both variables into account explicitly. The average values are now calculated along skewed lines with a slope determined by the ratio of the errors.

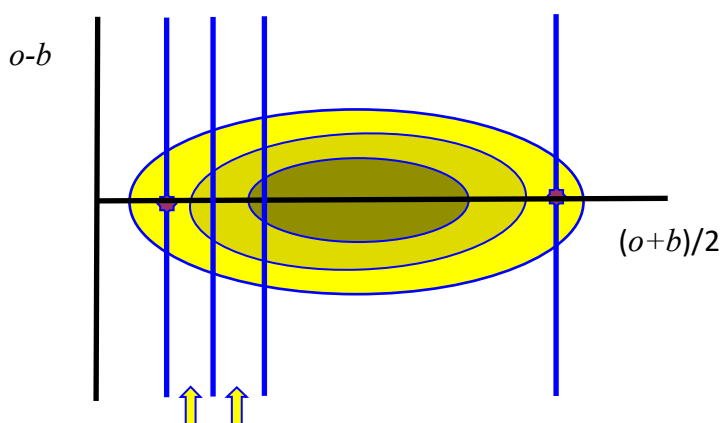


Figure 6 Bivariate  $o$  and  $b$  distribution, depicting the mean  $o - b$  as a function of  $(o + b)/2$  (red dots).

### 3.4 CDF matching

*Stoffelen* (1998b) used a technique for obtaining higher order calibration that is now commonly referred to as CDF matching, where CDF is the Cumulative probability Density Function of a variable. It follows from eq. (6) that two linearly calibrated collocated data sets (so  $a = 1$  and  $b = 0$ ) have identical underlying PDF of  $t$ . If both error PDFs are the same, both distributions must have identical CDF too. Since the CDF is a monotonically rising function, the CDFs of the two data sets may be mapped onto each other. This implies a higher order calibration of the two data sets, similar to what is obtained by binning  $o - b$  against  $o + b$ . *Stoffelen et al.* (2017) employ such method to obtain a scatterometer Geophysical Model Function (GMF), called CMOD7, with consistent response at all incidence angles used by the ERS and ASCAT scatterometers.

Thus CDF matching requires that both data sets have the same error variance. This will in general not be the case, but the error variances can be made equal if one assumes that the errors are Gaussian. Then, if  $\varepsilon_o^2 < \varepsilon_b^2$ , one can add a simulated Gaussian error with variance  $\varepsilon_b^2 - \varepsilon_o^2$  to the scatterometer winds. If  $\varepsilon_b^2 < \varepsilon_o^2$ , one can add a simulated Gaussian error with variance  $\varepsilon_o^2 - \varepsilon_b^2$  to the background. In both cases the two data sets should have equal error and true variance, so one can calculate the CDF's and match them, irrespective of the underlying true value distribution.

The values of  $\varepsilon_o^2$  and  $\varepsilon_b^2$  can be obtained from triple collocation. However, the triple collocation results are averages over all wind speeds and all WVC's. Plotting  $\varepsilon_{o-b}^2 = \varepsilon_o^2 + \varepsilon_b^2$  as a function of  $o + b$  will reveal variations of the total variance with average wind speed and /or WVC number. The error variances can now be made equal for each  $o + b$  bin and/or WVC number. This requires additional assumptions on  $\varepsilon_o^2$  or  $\varepsilon_b^2$ . One expects particularly  $\varepsilon_o$  to vary with WVC and  $\varepsilon_b$  to be rather independent of WVC. ERS and ASCAT errors are rather constant, but Ku-band scatterometer random errors depend on swath position and biases are known to depend on SST (*Wang et al., 2016*).

### 3.5 Geographical differences

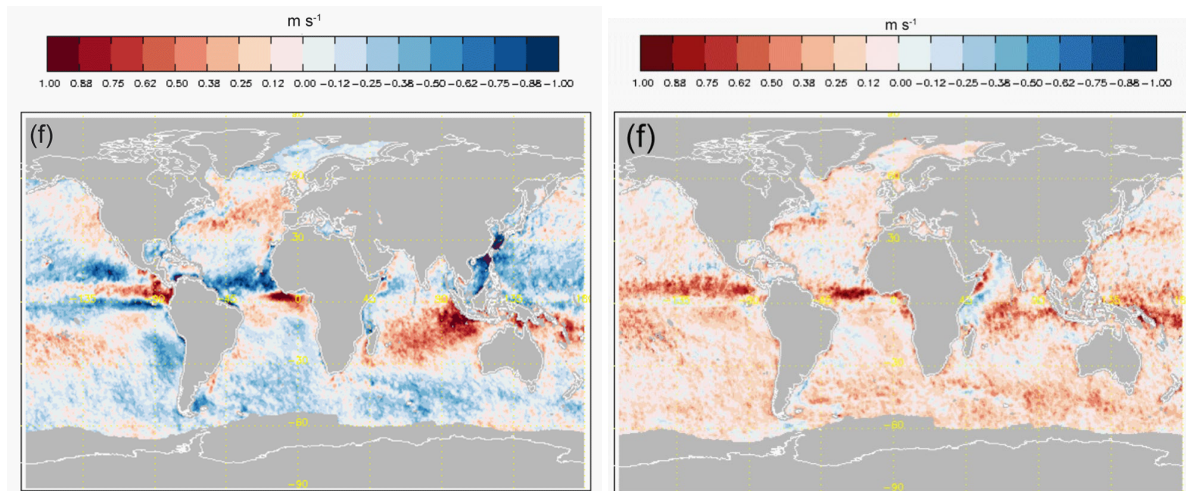


**Figure 7** Annual mean differences between ASCAT and collocated ECMWF ERA5 meridional stress-equivalent 10-m winds (left) and global maps of annual mean transient (eddy) meridional wind component differences between ASCAT and ERA5 (right) for 2016, from *Belmonte&Stoffelen (2019)*.

*Belmonte&Stoffelen (2019)* used stress-equivalent winds to compute monthly mean and monthly temporal (transient) variance maps for ASCAT and ERA5. Figure 7 shows meridional wind component differences for the mean and its variance for the whole year of 2016. These difference patterns tend to be rather persistent from year to year and slowly evolve over the seasons, months and days. Typical  $o-b$  wind component differences for ASCAT are 1.5 m/s in standard deviation and in amplitude quite comparable to some of the annual biases in mean and variance in the plot (cf. Table 2). This implies that the assumption of BLUE data

assimilation is locally violated, even after global calibration of ASCAT winds to ERA5. It indicates in practice that in some regions the innovations will be largely due to systematic model errors and the information on mesoscale weather contained in the scatterometer winds will essentially be lost in the process of data assimilation. Variational bias correction schemes, as already used for the assimilation of radiances, should be developed and employed in order to optimize the assimilation of scatterometer data.

NWP models deviate systematically from calibrated scatterometer winds due to (*Belmonte&Stoffelen, 2019*):

- 1) Air-sea interaction parameterization errors, e.g., the link between SST and wind gradients;
- 2) Marine Atmospheric Boundary Layer closure, particularly the stable MABL;
- 3) Representation of mesoscale phenomena, such as moist convection;
- 4) Mesoscale dissipation of 3D turbulence; NWP model dynamical closure;
- 5) Ocean currents, particularly for the zonal (equatorial) component.

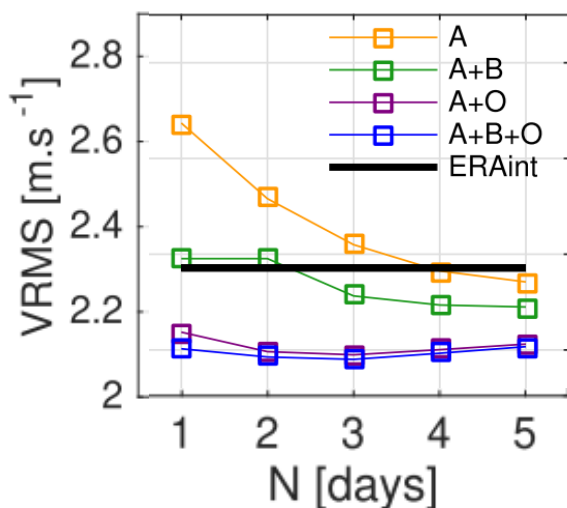


**Figure 8** Estimated vector root-mean-square (VRMS in  $\text{m.s}^{-1}$ ) difference between different ERAi/ERA\*  $U_{10s}$  products and independent HY2A scatterometer (HSCAT) ascending passes as a function of the temporal window size (N), over an 8 day period and latitudes  $[-55^\circ$  to  $55^\circ]$ . The different color lines show the VRMS scores for ERA-interim (black line in bold), ERA\* configuration using only ASCAT-A (orange line), ERA\* using ASCAT-A and B (green line), ERA\* using ASCAT-A and OSCAT (purple), and ERA\* using all of ASCAT-A, ASCAT-B, and OSCAT (blue).

### 3.5.1 ERA\*

*Trindade et al. (2020)* further investigated the persistency of the wind component biases over time. Based on  $o-b$  differences of several scatterometers, the locally average wind component biases were computed over several days, cf. Figure 8. Subsequently, these local biases were subtracted from the independent HY2A scatterometer (HSCAT) local  $o-b$  differences at the centre time of the averaging window. Note that such VARBC reduces  $o-b$  substantially by 10% for ERA-interim, in particular when 2 or 3 scatterometers are available. Moreover, the reduction is rather stable in time over several days, cf. the findings of *Belmonte&Stoffelen (2019)*. The corrected gridded ERA-interim model fields at every model time step are called ERA\* and will provide a physically more reliable ocean forcing stress. Given the stability of the corrections over several days, a local VARBC using past and current scatterometer winds will enable  $o-b$  bias correction and hence BLUE for scatterometer data assimilation.

Local VARBC corrections would encapsulate all model errors described above implicitly and may be associated to these. Acknowledging this may initiate a cycle of model error quantification, model improvement, air-sea coupling diagnostics and reduction of the VARBC corrections over time due to these improvements. Note, however, that such cycle is quite complex and may take many years. Some of the errors noted above have been known since a few decades, but their correction is linked to other errors in the modelling system.

In conclusion, geographical biases are substantial on all time scales and prevent BLUE. A local VARBC will remedy these biases and its adoption should be beneficial.

### 3.6 *Extreme Winds*

The availability of a reliable in-situ wind reference aids both satellite wind calibration and NWP modelling in extremes. However, in-situ wind speed references from moored buoys and dropsondes are inconsistent in their overlapping range from 15-25 m/s. NWP models need coupling to the ocean surface, which is generally arranged by specifying a wind drag coefficient. Inconsistencies in 10-m wind reference are associated with an uncertainty in this (NWP model) drag coefficient. Further note that different satellite wind products are now calibrated differently for extreme winds and are in fact mutually inconsistent. This problem is being elaborated in the international satellite winds community (e.g., in the EUMETSAT [CHEFS](#) project).

Dedicated hurricane campaigns are conducted to calibrate extreme scatterometer winds (e.g., *Esteban et al.*, 2006; *van Zadelhoff et al.*, 2014), where dropsondes are the main calibration standard in operations, for both satellite wind calibration and NWP model drag parameterizations. Dropsonde measurements have a large spread with respect to other wind references. ASCAT winds at KNMI have been developed using moored buoy in-situ wind speed as calibration reference. These winds deviate from dropsondes in the range above 15 m/s. However, reliable buoy measurements for calibration exist up to 25 m/s. At 25 m/s ASCAT wind speeds, dropsonde winds are estimated to be more than 10 m/s higher in the EUMETSAT CHEFS project (see Figure 9).

Winds derived from vertical polarization measurements, such as ASCAT winds, appear reliable up to 40 m/s on the dropsonde wind speed scale. Pencil-beam Ku-band scatterometers measure in horizontal polarization too and therefore more reliably represent extreme winds in hurricanes in the absence of rain.

Moored buoy wind sensors are calibrated at dedicated sites and in wind tunnels. Buoy winds are not frequent in hurricanes, but are validated by masts to be unbiased up to 25 m/s (within ~10%), while at 25 m/s the conversion bias in Figure 9d is 45%. Nevertheless, the buoy measurement platform and its interaction with large waves may cause failure to accurately determine extreme winds above 25 m/s (*Edson et al.*, 2018). Other in-situ (incl. land-based) wind sources suffer from wind flow distortion biases, both positive or negative, or from potentially systematic down-conversion errors to 10-m height.

---

Dropsondes cannot follow the wind near the surface, due to the strong deceleration as function of the drag. The implemented correction for this leads to an integration effect in the vertical, where the wind profile is logarithmic, and hence results in bias. This may contribute to the fact that 10-m dropsonde winds in hurricanes are inconsistent with a log profile. The position computation by the dropsonde GPS chip has not (yet) been investigated, nor its derivation of speed and acceleration, which are needed to compute 10-m wind and where inaccuracies may cause further bias in the strong deceleration (drag) near the surface ([CHEFS](#)).

Most passive satellite winds, SFMR, best track, Dvorak, etc. are all calibrated with respect to dropsondes and hence show the same inconsistency with respect to the buoy winds. Platform winds can also be scaled to such calibration reference (*Manaster et al., 2019*), but suffer from down-scaling biases and flow distortion. The conversion in Figure 9d takes the spatio-temporal scale of the verification sources into account, hence the deviation from the 1:1 line is not believed to be dominated by local spatial gradient effects.

The CHEFS project results call for further investigation of a consolidated in-situ wind speed reference in hurricane conditions. Due to the above-mentioned inconsistency, calibration of active and passive satellite winds (above 25 m/s) is uncertain, as well as their assimilation in NWP and the associated drag formulation in Earth System Models.

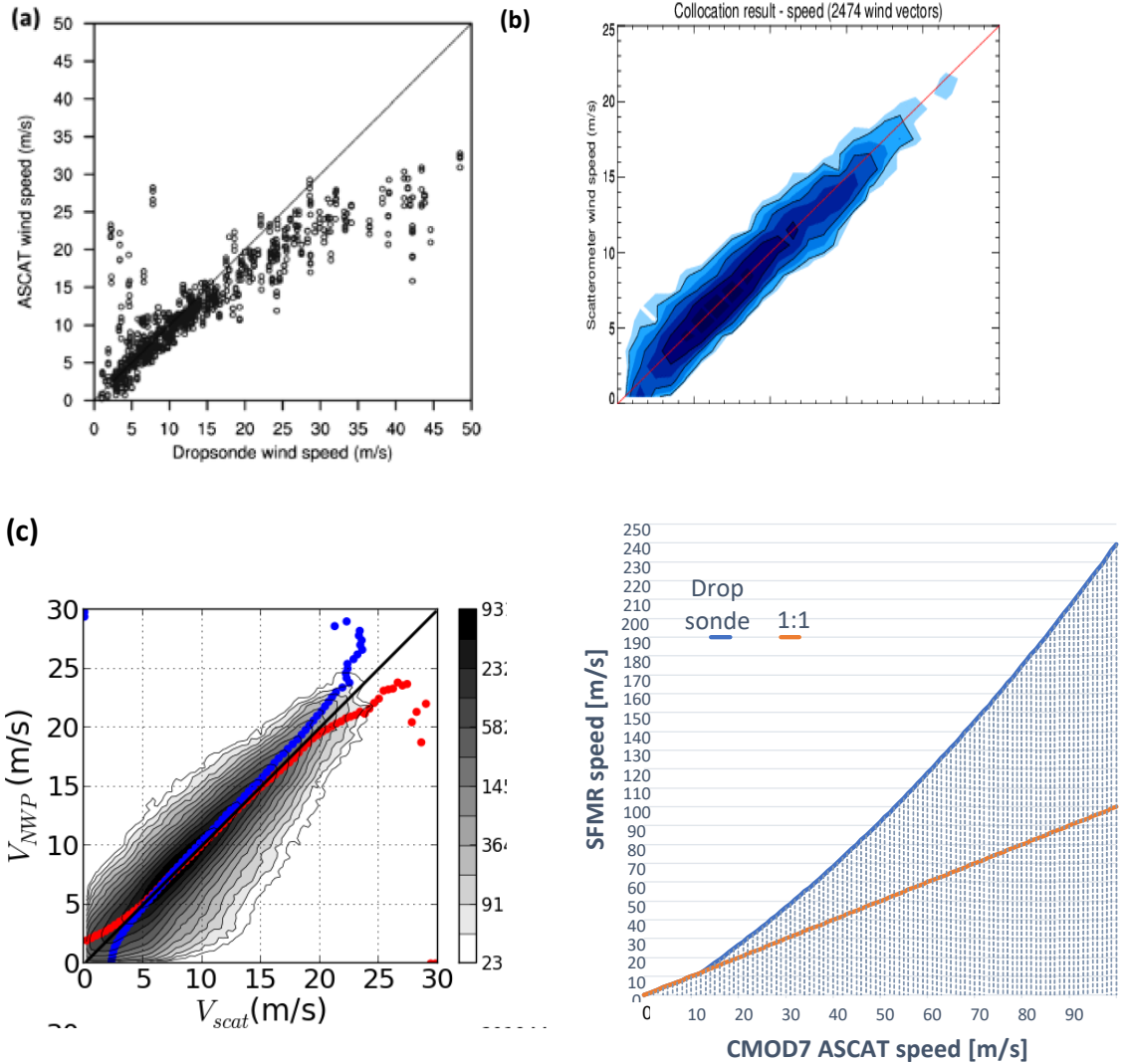


Figure 9 ASCAT wind speed scatter plots of a) ASCAT versus dropsondes (from *Chou et al., 2013*), b) ASCAT versus moored buoy winds and c) ECMWF NWP winds versus ASCAT. (d) depicts SFMR speeds, based on dropsonde calibration, versus ASCAT speeds, based on moored buoys ([CHEFS](#)).

## 4 Guidance

The output of NWP SAF wind data processors (including the OSI SAF wind products) is calibrated against in-situ wind data using triple collocation. Scatterometer winds are verified to be accurate and reliable and their assimilation is beneficial. Moreover, a golden age of scatterometry is emerging and improvements in data assimilation will be profitable.

Global NWP model wind climates may differ in quality and effective resolution and have rather large regionally-dependent biases that depend on NWP model closure of the dynamical equations, air-sea parameterization errors and lack of 3D turbulence and moist convection dynamics (*Belmonte&Stoffelen, 2019*). Regional models may also have such biases, lack mesoscale initialization over the oceans, but may also be affected by flow regime and boundary conditions (no mesoscale 3D turbulence at inflow boundaries for example). The long-term mean and transient variance biases in global NWP winds are locally of a size comparable to the  $o-b$  SD. Therefore, the BLUE paradigm is violated in scatterometer data assimilation. *Trindade et al. (2020)* suggest that local VARBC model state corrections aggregated over several days may reduce  $o-b$  SDs by about 15%, which is very substantial. Implementation of a VARBC to correct model errors and better guarantee BLUE data assimilation hence appears rather worthwhile.

At the same time, the scatterometer correction fields and their variances should be further investigated to link them to dynamical closure errors, sub-scale processes, such as moist convection, MABL organization, and ocean (eddy) interactions, to revisit their parameterization in NWP models. The current golden era of wind scatterometry will be helpful in this respect.

Since NWP model biases against observations are encountered, we recommend the following measures for an optimal scatterometer data assimilation:

- Recalibrate the scatterometer winds using the triple collocation and/or  $o - b$  regression techniques described above. In case of  $o - b$  regression, it is advised to calibrate the observations w.r.t. to the model, even when the model is known to be incorrect, to ensure model consistency in BLUE data assimilation. Regression (or CDF matching) will be adequate when the scatterometer observation  $U_{10S}$  error is similar to the NWP model  $U_{10S}$  error. The latter is NWP-model dependent, where NWP models encapsulating smaller spatial scales will generally have larger wind errors, due to lack of initialization of the small scales (see note <sup>2</sup> on page 20);
- Develop and employ a spatial and temporally slow-evolving (few days) variational bias correction in order to profit optimally (BLUE) from the accurate instantaneous dynamical information provided by scatterometers;
- Employ scatterometer-based NWP model  $U_{10S}$  bias and variability corrections for sea state and ocean forcing; this appear particularly relevant for ocean-atmosphere coupling;
- Improve model physics in order to better describe the reality as it is measured and/or correct the NWP model climate. However, this is not straightforward, since it depends on

many aspects and affects weather predictability (e.g., *Sandu et al.*, 2013). This is generally a longer term measure;

- Filter the data. If the problems occur at certain wind speed ranges, in certain geographical areas, or in certain times of the year, one may consider rejecting those data that cause problems. In this respect, we recommend to follow the quality control flags as set in the SAF wind processors, AWDP and PenWP, which are set to flag the most variable wind conditions, which are generally difficult to track in space and time.

Joint observation and NWP model wind distributions are known to be seasonally dependent and it is recommended to perform general PDF calibration tests with a data set representative of a full year.

Monitoring of  $o - b$  and  $o - a$  differences is needed to be reassured of constant NWP model wind climates. For examples of monitoring diagnostics we refer to the web links at the end of this document. Spatial analyses of comparison data sets which are collocated are recommended to compare identical weather samples of, e.g., NWP and scatterometer winds and therefore avoid effects of QC and sampling. Spatial characterization and comparison of OSE experiments based on non-collocated data sets leads to errors in interpretation, as the 3D turbulence spectrum on the mesoscales varies naturally by about one order of magnitude (*Nastrom and Gage*, 1985), such that QC decisions can have rather large statistical impact.

Geographical biases must be verified after calibration and need correction to ideally suit BLUE. Procedures for correction of persistent biases are being investigated by the OSI SAF team at KNMI: [scat@knmi.nl](mailto:scat@knmi.nl).

---

## References

Alpers, Werner, Biao Zhang, Alexis Mouche, Kan Zeng, Pak Wai Chan, 2016, Rain footprints on C-band synthetic aperture radar images of the ocean - Revisited, *Remote Sensing of Environment* 187, 169-185, ISSN 0034-4257, <https://doi.org/10.1016/j.rse.2016.10.015>.

Bidlot J.-R., D. J. Holmes, P. A. Wittmann, R. Lalbeharry, and H. S. Chen, 2002. Intercomparison of the performance of operational ocean wave forecasting systems with buoy data. *Wea. Forecasting* **17**, 287-310.

Chelton, D. and Q. Song, 2008. Observations and modeling of SST influence on surface winds. *ECMWF Workshop on Atmosphere-Ocean Interaction*, 10-12 November 2008. [http://www.ecmwf.int/newsevents/meetings/workshops/2008/ocean\\_atmosphere\\_interaction/presentations/index.html](http://www.ecmwf.int/newsevents/meetings/workshops/2008/ocean_atmosphere_interaction/presentations/index.html)

Chou, K.-H., C.-C. Wu, and S.-Z. Lin (2013), Assessment of the ASCAT wind error characteristics by global dropwindsonde observations, *J. Geophys. Res. Atmos.*, 118, 9011–9021, <dx.doi.org/10.1002/jgrd.50724>.

Dee, D., 2005. Bias and Data Assimilation. ECMWF/NWP-SAF Workshop on Bias estimation and correction in data assimilation, 8 - 11 November 2005.

Dee, D. and S. Uppala, 2008. Variational bias correction in ERA-Interim. ECMWF Technical Memorandum 575. <http://www.ecmwf.int/publications/library/do/references/list/14>

Edson, James, Doug Vandemark and Marc Emond, 2018, Evaluating several key issues in satellite wind stress validation, Int. Ocean Vector Winds Sc. Team IOVWST, Barcelona, Spain, [https://mdc.coaps.fsu.edu/scatterometry/meeting/docs/2018/docs/WednesdayApril25/WednesdayMorning/vandemark\\_edson\\_OVW2018\\_talk.pptx](https://mdc.coaps.fsu.edu/scatterometry/meeting/docs/2018/docs/WednesdayApril25/WednesdayMorning/vandemark_edson_OVW2018_talk.pptx).

Fois, F., 2015, Enhanced Ocean Scatterometry, PhD thesis Civil Engineering and Geosciences TU Delft, the Netherlands, <https://doi.org/10.4233/uuid:06d7f7ad-36a9-49fa-b7ae-ab9dfc072f9c>

Hersbach, H., 2010a. Comparison of C-band scatterometer CMOD5.N equivalent neutral winds with ECMWF, *J. Atm. Ocean. Tech.* **27**, 721-736. doi: 10.1175/2009JTECHO698.1

Hersbach, H., 2010b. The use of scatterometer winds at ECMWF, IOVWST presentation, [http://coaps.fsu.edu/scatterometry/meeting/docs/2010\\_may/gridded/hersbach.pdf](http://coaps.fsu.edu/scatterometry/meeting/docs/2010_may/gridded/hersbach.pdf)

Hersbach, H. and J. Bidlot, 2008. The relevance of ocean surface current in the ECMWF analysis and forecast system. *ECMWF Workshop on Atmosphere-Ocean Interaction*, 10-12 November 2008.

Kelly, K. A., S. Dickinson, M.J. McPhaden, and G. C. Johnson, 2001. Ocean currents evident in satellite wind data. *Geophys. Res. Lett.*, **28**, 2469-2472.

King, Gregory P., Marcos Portabella, Wenming Lin, and Ad Stoffelen, 2017, Correlating extremes in wind and stress divergence with extremes in rain over the Tropical Atlantic, Ocean and Sea Ice SAF Scientific Report OSI\_AVS\_15\_02 (v1.0).

King, Gregory P., Jur Vogelzang, and Ad Stoffelen, 2015. Upscale and downscale energy transfer over the tropical Pacific revealed by scatterometer winds, *J. Geophys. Res. Oceans*, **120**, doi: 10.1002/2014JC009993.

Kloe, J. de, A. Stoffelen and A. Verhoef, "Improved Use of Scatterometer Measurements by Using Stress-Equivalent Reference Winds, *IEEE J. Sel. Topics in Applied Earth Observ. and Rem. Sens.* **10** (5), 2340-2347, May 2017, doi: 10.1109/JSTARS.2017.2685242.

Lin, W., M. Portabella, A. Stoffelen, A. Turiel, and A. Verhoef, 2014. Rain Identification in ASCAT Winds Using Singularity Analysis. *IEEE Geosc. Rem. Sens. Lett.*, **11** (9), 1519-1523, doi: 10.1109/LGRS.2014.2298095

Lin, Wenming, Marcos Portabella, Ad Stoffelen, Jur Vogelzang, and Anton Verhoef, 2015. ASCAT wind quality under high sub-cell wind variability conditions. *Submitted to J. Geophys. Res.*

Manaster, A., Ricciardulli, L., & Meissner, T. (2019). Validation of High Ocean Surface Winds from Satellites Using Oil Platform Anemometers, *J. of Atmosph. and Oceanic Technol.* **36**(5), 803-818. <https://journals.ametsoc.org/view/journals/atot/36/5/jtech-d-18-0116.1.xml>.

Nastrom, G.D. and K.S. Gage, 1985. A climatology of atmospheric wavenumber spectra of wind and temperature observed by commercial aircraft. *J. Atm. Sci.*, **42**, 950-960.

Nie, Congling and D.G. Long, 2008. A C-Band scatterometer simultaneous wind/rain retrieval method. *IEEE Trans. Geosci. Rem. Sens.* **46** (11), 3618-3631, doi: 10.1109/TGRS.2008.922146.

Portabella, M., 2002. *Wind field retrieval from satellite radar systems*, Thesis University of Barcelona, Barcelona, Spain, 207p., [http://www.knmi.nl/publications/fulltexts/phd\\_thesis.pdf](http://www.knmi.nl/publications/fulltexts/phd_thesis.pdf)

Portabella, M. and A. Stoffelen, 2006, Scatterometer backscatter uncertainty due to wind variability. *IEEE Trans. Geosci. Rem. Sens.* **44** (11), 3356-3362, doi:10.1109/TGRS.2006.877952.

Portabella, M. and A. Stoffelen, 2009. On scatterometer ocean stress. *J. Geophys. Res.* **26**, 368-382.

Portabella, M., A. Stoffelen, W. Lin, A. Turiel, A. Verhoef, J. Verspeek and J. Ballabrera-Poy, 2012. Rain effects on ASCAT-retrieved winds: toward an improved quality control. *IEEE Trans. Geosc. Rem. Sens.*, **50** (7), 2495-2506, doi:10.1109/TGRS.2012.2185933.

Sandu, I., A. Beljaars, P. Bechtold, T. Mauritsen, and G. Balsamo, Why is it so difficult to represent stably stratified conditions in numerical weather prediction (NWP) models?, *J. Adv. Model. Earth Syst.*, **5**, 117–133, doi:10.1002/jame.20013.

Skamarok W. 2004. Evaluating NWP models using kinetic-energy spectra. *Mon. Weather Rev.* **132**, 3019–3032.

Stoffelen, Ad, Jur Vogelzang and Gert-Jan Marseille, 2020, High-resolution wind data-assimilation guide, EUMETSAT docs. SAF/OSI/CDOP3/KNMI/SCI/GUI/388 or NWPSAF-KN-UD-008, v1.3, KNMI, De Bilt, The Netherlands,

Stoffelen, Ad, J. A. Verspeek, J. Vogelzang and A. Verhoef, 2017, "The CMOD7 Geophysical Model Function for ASCAT and ERS Wind Retrievals," in IEEE Journal of Selected Topics in Applied Earth Observations and Remote Sensing, vol. 10, no. 5, pp. 2123-2134, doi: 10.1109/JSTARS.2017.2681806.

Stoffelen, Ad, Jur Vogelzang, and Wenming Lin, 2015, On buoys, scatterometers and reanalyses for globally representative winds, Technical report NWPSAF-KN-TR-024, version 1.1, 28-8-2015, NWP SAF, [www.nwpsaf.eu/publications/tech\\_reports/nwpsaf-kn-tr-024.pdf](http://www.nwpsaf.eu/publications/tech_reports/nwpsaf-kn-tr-024.pdf)

Stoffelen, A. and M. Portabella, 2006. On Bayesian scatterometer wind inversion, *IEEE Trans. Geosci. Rem. Sens.* **44** (6), 1523-1533.

Stoffelen, A., 1998a. *Scatterometry*, PhD thesis, University Utrecht, <http://igitur-archive.library.uu.nl/dissertations/01840669/inhoud.htm>

Stoffelen, A., 1998b. Toward the true near-surface wind speed: error modeling and calibration using triple collocation, *J. Geophys. Res.* **103C**, 7755-7766.

Trindade, A., M. Portabella, A. Stoffelen, W. Lin and A. Verhoef, ERAstar: A High-Resolution Ocean Forcing Product, IEEE Transactions on Geoscience and Remote Sensing, 2020, 58, 2, 1337-1347, doi:10.1109/TGRS.2019.2946019.

Trindade, Ana, M. Portabella, W. Lin, A. Stoffelen and A. Verhoef, 2015, Towards the characterization and removal/mitigation of scatterometer wind sampling errors, IOVWST meeting, Portland, USA, May 2015, [coaps.fsu.edu/scatterometry/meeting/docs/2015/ClimateDataRecordDevelopmentAndAnalysis/Trindade IOVWST 2015 final.pdf](http://coaps.fsu.edu/scatterometry/meeting/docs/2015/ClimateDataRecordDevelopmentAndAnalysis/Trindade_IOVWST_2015_final.pdf)

Verhoef, Anton, Ad Stoffelen, Jeroen Verspeek, Jur Vogelzang, 2019, Wind Product User Manual, EUMETSAT Ocean and Sea Ice SAF/Advanced Retransmission Service document for ASCAT Global OSI SAF 25-km wind product (OSI-102, OSI-102-b, and OSI-102-c), Global OSI SAF 12.5 km wind product (OSI-103 - discontinued), Global OSI SAF coastal wind product (OSI-104, OSI-104-b, and OSI-104-c), Regional EARS 25-km wind product, Regional EARS coastal wind product, version 1.16, [scatterometer.knmi.nl/publications/pdf/ASCAT\\_Product\\_Manual.pdf](http://scatterometer.knmi.nl/publications/pdf/ASCAT_Product_Manual.pdf)

Vogelzang, J., and A. Stoffelen, 2017, "ASCAT Ultrahigh-Resolution Wind Products on Optimized Grids", IEEE Journal of Selected Topics in Applied Earth Observations and Remote Sensing 10(5), 2332-2339, doi: 10.1109/JSTARS.2016.2623861.

Vogelzang, J., A. Stoffelen, A. Verhoef, J. de Vries, and H. Bonekamp, 2009. Validation of two-dimensional variational ambiguity removal on SeaWinds scatterometer data. *J. Atm. Oceanic Technol.*, **7**, (26), 1229-1245, doi:10.1175/2008JTECHA1232.1.

---

Vogelzang, J., A. Stoffelen, A. Verhoef, and J. Figa-Saldaña, 2011. On the quality of high resolution scatterometer winds, *J. Geophys. Res.* **116**, C10033. doi: 10.1029/2010JC006640.

Wang, Z., Stoffelen, A., Zou, J., Lin, W., Verhoef, A., Zhang, Y., He, Y. and Lin, M., 2020. Validation of New Sea Surface Wind Products From Scatterometers Onboard the HY-2B and MetOp-C Satellites. *IEEE Transactions on Geoscience and Remote Sensing*, 58(6), pp.4387-4394.

Wang, Z., A. Stoffelen, C. Zhao, J. Vogelzang, A. Verhoef, J. Verspeek, M. Lin, and G. Chen, 2017, An SST-dependent Ku-band geophysical model function for RapidScat, *J. Geophys. Res. Oceans*, 122, 3461–3480, doi:10.1002/2016JC012619.

Xu, X. and A. Stoffelen, Improved Rain Screening for Ku-Band Wind Scatterometry, *IEEE Transactions on Geoscience and Remote Sensing*, 2020, 58, 4, 2494-2503, doi:10.1109/TGRS.2019.2951726.

Zadelhoff, G.-J. van, Ad Stoffelen, P. W. Vachon, J. Wolfe, J. Horstmann, and M. Belmonte Rivas, 2014, Atmospheric measurement techniques retrieving hurricane wind speeds using cross-polarization C-band measurements, *Atmospheric Measurement Techniques*, **7**(2) 437-449.

---

## Useful web sites

- NWP SAF monitoring pages:

[nwp-saf.eumetsat.int/site/monitoring/](http://nwp-saf.eumetsat.int/site/monitoring/)

- OSI SAF monitoring pages at KNMI:

[scatterometer.knmi.nl/osisaf/](http://scatterometer.knmi.nl/osisaf/)

Select a wind product on the right hand side of the screen and then “Monitoring information”, again on the right hand side of the screen.

- IOVWST meeting presentations:

[coaps.fsu.edu/scatterometry/meeting/](http://coaps.fsu.edu/scatterometry/meeting/)

Various presentations on calibration and applications.

- International Winds Working Group:

[groups.ssec.wisc.edu/groups/iwwg/activities/high-resolution-winds-1/nwp-data-assimilation](http://groups.ssec.wisc.edu/groups/iwwg/activities/high-resolution-winds-1/nwp-data-assimilation),

- Wind data assimilation workshop:

[scatterometer.knmi.nl/publications/pdf/Mesoscale\\_Wind\\_Assimilation\\_Ad\\_NWPSAF.pdf](http://scatterometer.knmi.nl/publications/pdf/Mesoscale_Wind_Assimilation_Ad_NWPSAF.pdf)

- References on data assimilation, scatterometry and quality aspects:

[scatterometer.knmi.nl/training\\_material/](http://scatterometer.knmi.nl/training_material/) and  
[scatterometer.knmi.nl/publications/](http://scatterometer.knmi.nl/publications/).